Real-time Performance Evaluation of Relative Calibration on the OAI 5G testbed

Theoni Magounaki
Orange Labs
Sophia Antipolis, France
theoni.magounaki@orange.com

Florian Kaltenberger
EURECOM
Sophia Antipolis, France
florian.kaltenberger@eurecom.fr

Raymond Knopp
EURECOM
Sophia Antipolis, France
raymond.knopp@eurecom.fr

***Abstract*—In this paper we describe the OpenAirInterface (OAI) C-RAN testbed deployed at Eurecom and present the real-time implementation and performance evaluation of a channel calibration scheme. The distributed MIMO operation in dense Time Division Duplex (TDD) radio networks requires accurate time and frequency synchronization and calibration for precoding. We achieve this by using a common reference and over-the-air (OTA) synchronization between remote radio units (RRUs), which is a much cheaper alternative to distributed synchronization using PTPv2-like protocols and special clock regeneration circuitry. Furthermore we perform channel measurements between the RRUs without interrupting the real-time operation in order to perform distributed channel reciprocity calibration which is required to exploit uplink (UL) channel estimates to infer the precoder performed on the downlink (DL) channel.**

***Index Terms*—channel reciprocity calibration, distributed antenna system, TDD, synchronization, C-RAN**

I. Introduction

Massive multiple input multiple output (mMIMO) is one of the most promising wireless physical layer technologies to address the massive capacity requirement demanded by 5G systems. Massive MIMO exploits the use of large antenna arrays at the base station (BS) to simultaneously serve multiple users through spatial multiplexing over a channel. mMIMO relies on uplink pilots to obtain channel state information (CSI), exploiting channel reciprocity and time division duplexing (TDD) operation.

Distributed mMIMO or distributed antenna system (DAS) with spatially separated antennas is considered for improving indoor coverage with not so large number of antennas [1]. Distributed multi-user MIMO (MU-MIMO) unifies small cells and mMIMO approaches. Simultaneously obtaining both multi-user interference suppression through spatial precoding, and dense coverage by reducing the average distance between transmitters and receivers. This is achieved by coordinating a large number of remote radio units (RRUs), distributed over a certain coverage region, through a wired backhaul network connected to a central server, in order to form a DAS.

One of the biggest challenges in such distributed massive MIMO networks is synchronization of the RRUs. The two common methods for radio synchronization are the *time-based synchronization* using a periodic pulse per second (PPS) and *trigger-based/signal synchronization* based on a shared trigger architecture. The periodic PPS signal, provided by various commercial off-the-shelf (COTS) GPS-disciplined oscillators (GPSDO), is used for establishing a common time base among the radios. The timed-based synchronization would require each time the system is started up a calibration procedure, controlled by a host controller, to establish a common time along RRUs. Moreover, the latency introduced by the clock cycled prevents the immediate triggering of any process. In our implementation we therefore choose trigger based synchronization as explained in Section III.

In the present paper, we present a group-based OTA calibration framework and through real-time measurements on our C-RAN testbed and OAI software we compare its performance against existing calibration algorithms. We show the performance gains when we minimize the size of the largest group and simultaneously forming groups by selecting RRUs in an interleaving way.

The rest of this paper is organized as follows. Section II describes the system architecture of our testbed. Section III explains the synchronization and calibration algorithms implemented. In Section IV, we present the TDD reciprocity system model and the fast calibration (FC) scheme based on antenna grouping. In Section V, we compare the performance of the group-based FC method with existing calibration schemes using variance as a metric. Conclusions are drawn in Section VI.

II. System Architecture

Eurecom deployed a cloud radio access network (C-RAN) network using OpenAirInterface (OAI) software and inexpensive commodity hardware, Fig. 1 [2]. The testbed consists of the following 3 main entities: (i) The remote radio unit (RRU) which is a radio transceiver and contains the RF processing circuitry. (ii) The radio aggregation unit (RAU) which connects multiple RRUs to a baseband unit (BBU) and serves as a data processing unit. (iii) The radio cloud center (RCC) which is responsible for the centralized baseband processing and controls multiple RAUs.

A set of 20 RRUs is deployed on the ceilings of the corridors on levels -3 and -4 of the Eurecom building. The RRUs on each floor are connected by Gbit Ethernet to a switch which

This work has been funded by the french project MASS-START and EU project 5G-Picture (H2020-ICT-2016-2)

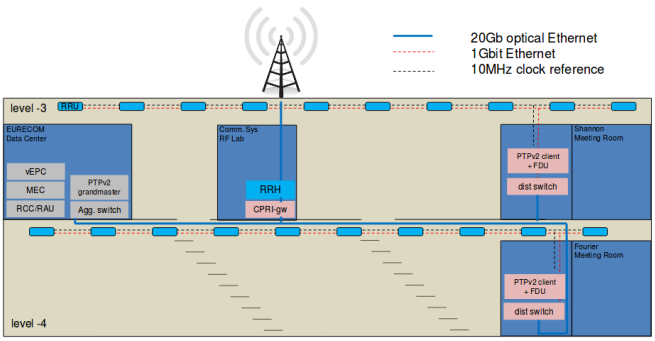

Fig. 1. OpenAirInterface 5G testbed

are in turn connected to a central server over optical 20 Gbit Ethernet. An additional high power commercial remote radio head (RRH) is connected to the C-RAN server through a common public radio interface (CPRI) gateway. A frequency reference unit outputs ten high-precision 10 MHz frequency reference outputs on each floor. The RRUs consist of an UP board from Intel, a B200 mini from Ettus Research, a RF frontend designed by Eurecom and Power over Ethernet (PoE) technology.

III. Synchronization and Calibration

There are three levels of synchronization: (i) time synchronization to ensure that the frames are aligned between the different RRUs up to within a sample, (ii) frequency synchronization to ensure that the RRUs stay synchronized in time and phase and (iii) phase synchronization to enable coherent transmission and precoding. Our system is based on LTE TDD configuration 1, which has two UL, two DL, and one special subframe every 5ms.

A. Time synchronization

Time across all RRUs must be synchronized to within the accuracy of 1 sample of the A/D and D/A converters.

Time synchronization is achieved by using over-the-air trigger-based synchronization using a "master-slave" protocol, where one RRU acts as the master the other RRU synchronize to it much as an UE would synchronize to the network. However, the primary synchronization sequence (PSS) used for UE synchronization would not provide the required accuracy as it only occupies $\sim$1MHz. Therefore we have added a demodulation reference symbol (DMRS) in OFMD symbol 3 of the special subframe 1, just after the PSS. As soon as the initial sync is done the frames are aligned and the slave RRUs start to connect to RAU. When the RAU knows that slave is running it sends a resynchronization command to the slave RRU to change its frame number to the right one.

B. Frequency Synchronization

In order to have all the RRUs form a single DAS, we have to provide a reference for frequency and time synchronization. A shared 10 MHz oven-controlled crystal oscillator (OCXO) reference provides frequency disciplining for the internal voltage-controlled oscillator (VCO) used to generate the system local oscillator (LO) and A/D and D/A channels, both of which must be synchronized across the entire RRU array.

Sharing the common 10 MHz reference among RRUs allows a phase-coherent LO to be synchronized using a fractional-N frequency approach. During synthesis, as the reference is divided, the phase may lock on either rising or falling edges producing a constant but arbitrary phase offset on each channel. Due to a poor PLL design on the B200 USRPs we realized that the phase does not lock, rendering our system beamforming-uncapable. To deal with this phase incoherence we disabled the VCTCXO at each RRU and we replaced it with a 40MHz signal which is directly fed into the RF chip of the B200.

C. Phase synchronization

Beamforming places additional requirements on the system. In addition to sample time and sample clock alignment, the system must maintain a known phase relationship between each RF chain. However, because each radio has an independent synthesizer circuit (PLL-VCO) for both Tx and Rx, the phase can be considered phase coherent but not phase aligned. Through periodic calibration, alignment can be achieved by digitally adjusting the real and imaginary signal component (I,Q) phase.

In order to calibrate the C-RAN testbed we need to collect channel measurements between the master and the slave RRUs. This is achieved by using the framework shown in Fig. 2. In this example there are 3 RRUs, 1 master RRU M and 2 slave RRUs S0,S1. In the first special subframe (SSF) in a TDD configuration 1 frame symbol 3 and 10 are reserved DMRS symbols. The slave RRUs sacrifice symbol 2 in order to switch from Tx to Rx mode, so that PSS is omitted and only the first two PDCCH symbols are transmitted in the DL. At each special subframe 1 every 10ms, only one RRU transmits the calibration symbol. If the RRU which is in transmit mode is a master RRU then all the active slave RRUs receive, decode and estimate the DL channel estimates at symbol 10. On the other side, if a slave RRU transmits the calibration symbol, only the master RRU collects and estimates the UL channel estimates. Thus, a bidirectional calibration symbol exchange for a pair of RRUs takes up to 20ms. We assign a number at each RRU, *tag*, such that each RRU enables its transmit mode if and only if $\mathit{frame} \bmod p = \mathit{tag}$, where $\mathit{frame} = \{0, 1, .., 1023\}$ is the frame number and p is the number of active RRUs in the testbed. In contrast to the frequency with which the master RRU transmits the calibration symbol, the synchronization symbol is broadcasted to the slave RRUs every 10ms.

After acquiring channel estimates between the master and slave RRUs we use the reciprocity calibration method described in the next section.

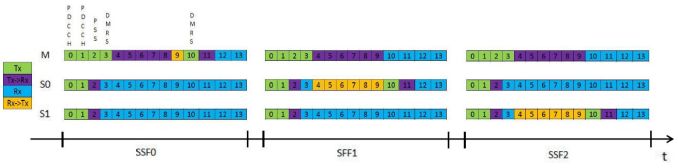

Fig. 2. Synchronization-Calibration framework

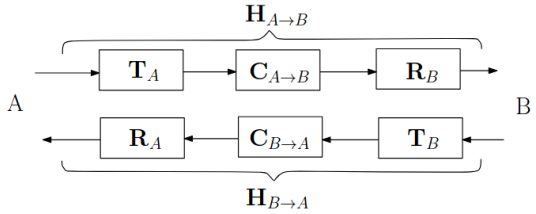

Fig. 3. Reciprocity Model

IV. Over-the-air reciprocity calibration in OAI C-RAN testbed

TDD reciprocity calibration and RRU synchronization are the two key factors to enable distributed multi-user MIMO. In this section we present the reciprocity calibration scheme from [3] applied to the C-RAN testbed. We further analyze the synchronization problems that arise in such a platform and we propose low-cost solutions.

A. Relative Calibration Scheme

We consider a TDD communication system involving a BS A and a UE B with M_A antennas and M_B antennas respectively, illustrated in Fig. 3. The channel seen by transceivers in the digital domain (the composite channel), is comprised of the physical channel $\mathbf{C}$, assumed reciprocal in both UL and DL, and filters modeling the imperfections of the transmit RF hardware (e.g., power amplifiers (PA)), ($\mathbf{T}_A$ and $\mathbf{T}_B$), and the receive RF hardware (e.g, low-noise amplifiers (LNA)), ($\mathbf{R}_A$ and $\mathbf{R}_B$). The diagonal elements represent the gains on each transmit chain whereas the off-diagonal elements correspond to the RF chain on-chip crosstalk and the antenna mutual coupling. We consider the ideal case, where the transmit/receive RF hardware are all diagonal filters (no crosstalk/mutual coupling) and carrier frequency at both sides is identical. Also, the filters modeling the amplifiers are assumed to remain constant over the observed quite long time horizon. The measured UL and DL channels between nodes A and B, represented by $\mathbf{H}_{A\to B}$ and $\mathbf{H}_{B\to A}$, are thus modeled as:

$$\begin{aligned}\boldsymbol{H}_{A\to B} &= \boldsymbol{R}_B\boldsymbol{C}_{A\to B}\boldsymbol{T}_A\\ \boldsymbol{H}_{B\to A} &= \boldsymbol{R}_A\boldsymbol{C}_{B\to A}\boldsymbol{T}_B\end{aligned} \tag{1}$$

Since we operate within the channel coherence time we can eliminate the physical channel $\mathbf{C}$ from (1) and we obtain:

$$\boldsymbol{H}_{A\to B} = \boldsymbol{F}_B^{-T}\boldsymbol{H}_{B\to A}^{T}\boldsymbol{F}_A \tag{2}$$

where $\boldsymbol{F}_A = \boldsymbol{R}_A^{-T}\boldsymbol{T}_A$ and $\boldsymbol{F}_B = \boldsymbol{R}_B^{-T}\boldsymbol{T}_B$ include the hardware properties and are called the *calibration matrices*.

OTA calibration relies on signal processing techniques to calibrate at RF chain level and compensate the hardware non-symmetry. Thus, we estimate $\boldsymbol{F}_A$ and $\boldsymbol{F}_B$ which along with the UL channel estimates $\boldsymbol{H}_{B\to A}$ give us the CSIT $\boldsymbol{H}_{A\to B}$, (2), based on which advanced beamforming techniques can be implemented. In [4] it is shown that the RF mismatches at the BS, and not at the UE side, are the major factor for degrading the system's performance. Hence, we perform *partial calibration* which is part of the relative or over-the-air (OTA) calibration methods. In partial calibration only the RF mismatches at the BS are calibrated. This has no impact at the beamforming performance as any unknown complex scalar factor is compensated by the channel estimation at the UE. We thus, in the sequel, focus on the estimation of $\mathbf{F}_A$, although the framework discussed in the following is not limited to this case.

Let as describe how the calibration matrix $\boldsymbol{F}_A$ is estimated based on the fast calibration scheme proposed in [3]. We consider a set of M RRUs partitioned into G groups denoted by $A_1, A_2, \ldots, A_G$, as in Fig. 4. Group A_i contains M_i RRUs such that $\sum_{i=1}^{G} M_i = M$. Each group A_i transmits a sequence of L_i pilot symbols, defined by matrix $\mathbf{P}_i \in \mathbb{C}^{M_i\times L_i}$ where the rows correspond to antennas and the columns to successive channel uses. A channel use is considered as a calibration symbol or a frame. When an antenna group i transmits, all other groups are considered in receiving mode. After all G groups have transmitted, the received signal for each resource block of bidirectional transmission between antenna groups i and j is given by

$$\begin{aligned}\mathbf{Y}_{i\to j} &= \mathbf{R}_j\mathbf{C}_{i\to j}\mathbf{T}_i\mathbf{P}_i + \mathbf{N}_{i\to j}\\ \mathbf{Y}_{j\to i} &= \mathbf{R}_i\mathbf{C}_{j\to i}\mathbf{T}_j\mathbf{P}_j + \mathbf{N}_{j\to i}\end{aligned} \tag{3}$$

where $\mathbf{Y}_{i\to j} \in \mathbb{C}^{M_j\times L_i}$ and $\mathbf{Y}_{j\to i} \in \mathbb{C}^{M_i\times L_j}$ are received signal matrices at antenna groups j and i respectively. $\mathbf{N}_{i\to j}$ and $\mathbf{N}_{j\to i}$ represent the corresponding received noise matrix. $\mathbf{T}_i$, $\mathbf{R}_i \in \mathbb{C}^{M_i\times M_i}$ and $\mathbf{T}_j$, $\mathbf{R}_j \in \mathbb{C}^{M_j\times M_j}$ represent the effect of the transmit and receive RF front-ends of antenna elements in groups i and j respectively.

The reciprocity property induces that $\mathbf{C}_{i\to j} = \mathbf{C}_{j\to i}^{T}$, thus for two different groups $1 \le i \ne j \le G$ in (3), by eliminating $\mathbf{C}_{i\to j}$ we have

$$\mathbf{P}_i^T\mathbf{F}_i^T\mathbf{Y}_{j\to i} - \mathbf{Y}_{i\to j}^T\mathbf{F}_j\mathbf{P}_j = \widetilde{\mathbf{N}}_{ij} \tag{4}$$

The calibration matrix $\mathbf{F}$ is diagonal and thus we can consider $\mathbf{F}_i = \mathrm{diag}\{\mathbf{f}_i\}$ and $\mathbf{F} = \mathrm{diag}\{\mathbf{f}\}$. This allows us to vectorize (4) into

$$(\mathbf{Y}_{j\to i}^T * \mathbf{P}_i^T)\mathbf{f}_i - (\mathbf{P}_j^T * \mathbf{Y}_{i\to j}^T)\mathbf{f}_j = \widetilde{\mathbf{n}}_{ij} \tag{5}$$

where $*$ denotes the Khatri–Rao product, where we have used the equality $\mathrm{vec}(\mathbf{A}\,\mathrm{diag}(\mathbf{x})\,\mathbf{B}) = (\mathbf{B}^T * \mathbf{A})\,\mathbf{x}$. Stacking equations (5) for all $1 \le i < j \le G$ yields

$$\boldsymbol{\mathcal{Y}}(\mathbf{P})\mathbf{f} = \widetilde{\mathbf{n}} \tag{6}$$

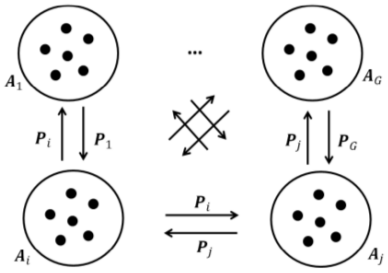

Fig. 4. Bi-directional transmission between antenna groups.

with $\boldsymbol{\mathcal{Y}}(\mathbf{P})$ defined as

$$\underbrace{\begin{bmatrix} (\mathbf{Y}_{2\to1}^T * \mathbf{P}_1^T) & -(\mathbf{P}_2^T * \mathbf{Y}_{1\to2}^T) & 0 & \dots \\ (\mathbf{Y}_{3\to1}^T * \mathbf{P}_1^T) & 0 & -(\mathbf{P}_3^T * \mathbf{Y}_{1\to3}^T) & \dots \\ 0 & (\mathbf{Y}_{3\to2}^T * \mathbf{P}_2^T) & -(\mathbf{P}_3^T * \mathbf{Y}_{2\to3}^T) & \dots \\ \vdots & \vdots & \vdots & \ddots \end{bmatrix}}_{(\sum_{j=2}^{G}\sum_{i=1}^{j-1} L_i L_j)\times M} \tag{7}$$

The estimation of the calibration coefficients $\mathbf{f}$ consists in solving a LS problem assuming a unit norm constraint such as

$$\hat{\mathbf{f}} = \arg\min_{\mathbf{f}:\|\mathbf{f}\|=1} \|\boldsymbol{\mathcal{Y}}(\mathbf{P})\,\mathbf{f}\|^2 \;=\; V_{min}(\boldsymbol{\mathcal{Y}}(\mathbf{P})^H \boldsymbol{\mathcal{Y}}(\mathbf{P})) \tag{8}$$

where $V_{min}(\mathbf{X})$ denotes the eigenvector of matrix $\mathbf{X}$ corresponding to its eigenvalue with the smallest magnitude.

V. Experimental Results

In this section, results from the experimental measurements are presented to illustrate the efficient application of the proposed fast calibration (FC) scheme to our real-time C-RAN testbed. The DL/UL channel estimates extracted from the DMRS calibration symbols are sent via packetized I/Q samples to the RAU over fronthaul protocol on commodity Ethernet. The RAU receives inter-RRU reference signal measurements and deduces the needed calibration information to form a distributed MIMO transmitter. The system has always to be under calibrated status, therefore, calibration procedures need to be repetitively performed.

We first compare the proposed group-based FC method from Section IV against the existing calibration methods Argos [5], Rogalin [6], [7], [8] and Avalanche [9]. FC-2-2-1 and FC-3-2 correspond to two different grouping schemes in the case of a set of $M = 5$ RRUs and FC-I corresponds to a fast calibration scheme where the RRU grouping is exactly the same as that of Avalanche (i.e., 1-1-2-1). We assess numerically the performance of various calibration algorithms and compare them based on how spread out the data set is.

Fig. 5 depicts the diagonal estimation of the calibration matrix $\hat{\mathbf{f}}_j[l,k]$, in which each circle is composed of $k = 1,\dots,600$ subcarriers covering the whole bandwidth, for each RRU with tag j, through $l = 1,\dots,L$ measurements. Note that the first coefficients are fixed to 1 so that $\mathbf{f}_1 = 1$. Converting

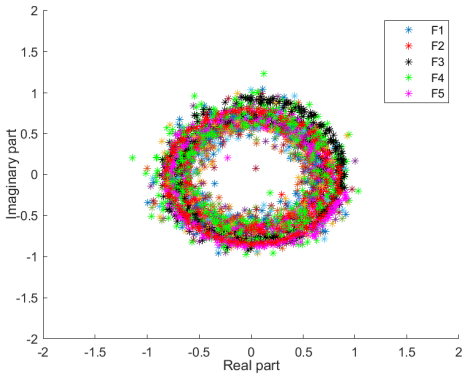

Fig. 5. Calibration coefficients in frequency domain using group-based FC method.

the frequency response to the time domain using (9) we can see in Fig. 6 that a single filter tap is sufficient to represent the channel.

$$\hat{\mathbf{g}}_j[l,k] = \underset{k}{\mathrm{IFFT}}\{\hat{\mathbf{f}}_j[l,k]\} \tag{9}$$

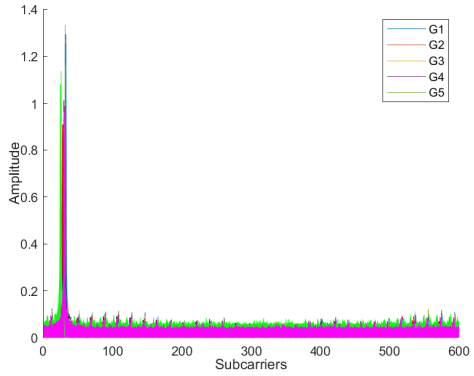

Fig. 6. Calibration coefficients in time domain.

Thus, we compute the variance of the time-domain calibration elements computed at the maximum value given by

$$\begin{aligned} k' &= \arg\max_{k} \hat{\mathbf{g}}_j[l,k], \\ \tilde{\mathbf{g}}_j &= \underset{l}{var}(\hat{\mathbf{g}}_j[l,k']). \end{aligned} \tag{10}$$

In Fig. 7 the performance of the proposed FC-2-2-1 grouping greatly outperforms that of the Avalanche scheme. The LS estimator in Avalanche uses previously estimated calibration parameters which causes error propagation; estimation errors on a given calibration coefficient will propagate to subsequently calibrated RRUs. Moreover, it is important to note that the performance with the FC-2-2-1 grouping improves dramatically compared to the FC-3-2 scheme, since the overall estimation performance of the group-based FC is limited by the condition number of the largest group size. Hence, it is reasonable to try to minimize the size of the largest RRU group.

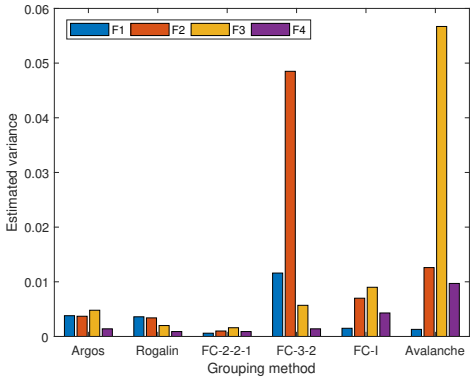

Fig. 7. Variance of the time-domain calibration coefficients (computed at the maximum value) for M=5.

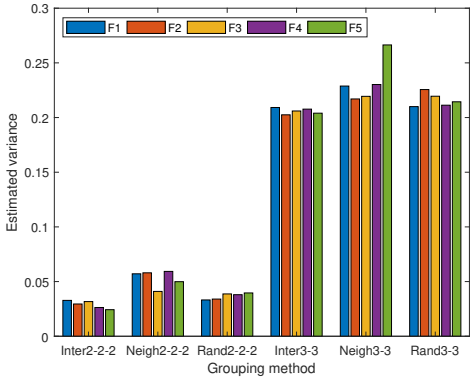

Fig. 8. Comparison of three different choices to form the RRU groups (FC with equally partitioned groups, M=6).

Fig. 8 illustrates the performance results from three different grouping schemes (Interleaved, Neighbours, Random). "Interleaved" grouping corresponds to selecting every other RRU along to corridor while "Neighbours" scheme groups the closest RRUs together, Fig. 9. The performance gains at Inter2-2-2 and Inter3-3 show that the interleaving of the RRUs ensures that the channel from a group to the rest of the RRUs is as well conditioned as possible. Furthermore, we verify the fact that the performance improves when the group sizes are allocated more equitably to the minimum group size as in grouping scheme Inter2-2-2 which has a lower condition number (well-conditioned) than for scheme Inter3-3. A condition number applies to the LS problem being solved in (7). We invert the matrix, finding its eigenvalues. In Inter3-3 scheme, the matrix can be poorly conditioned for inversion so it is more sensitive to machine's relative round-off errors made during the LS solution process.

VI. Conclusions

In this work we presented an OTA calibration framework and through real-time measurements on our C-RAN testbed and OAI software, we performed distributed channel reciprocity calibration. We achieved to maintain OTA synchronization between several RRUs and confirmed the efficiency of the proposed fast calibration schemes based on RRU grouping in real environment. Our results illustrated that the FC with equally partitioned groups outperforms the existing Argos, Rogalin and Avalanche methods. Moreover, we presented the case where the overall estimation performance of our FC algorithm improves when we try to minimize the size of the largest RRU group. Finally, we proved through real-time measurements that the interleaved grouping of the RRUs results in performance gains.

Next step will be to integrate the group-based FC method into the communications part with UEs and perform some beamforming techniques on our C-RAN testbed.

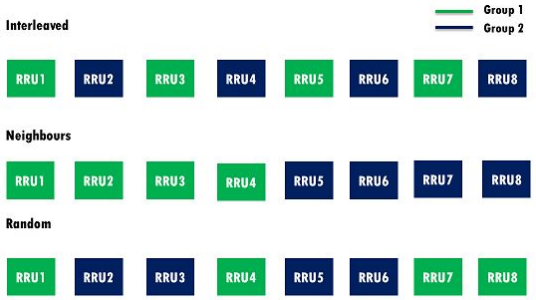

Fig. 9. Example of three different choices to form the RRU groups for M=8 RRUs.

References

[1] A. A. M. Saleh, A. Rustako, and R. Roman, "Distributed antennas for indoor radio communications," *IEEE Transactions on Communications*, vol. 35, no. 12, pp. 1245–1251, December 1987.

[2] F. Kaltenberger, X. Jiang, and R. Knopp, "From massive MIMO to C-RAN: the OpenAirInterface 5G testbed," in *Proceeding of Asilomar Conference on Signals, Systems, and Computers*, Pacific Grove, CA, Oct. 2017.

[3] X. Jiang, A. Decunringe, K. Gopala, F. Kaltenberger, M. Guillaud, D. Slock, and L. Deneire, "A framework for over-the-air reciprocity calibration for TDD massive MIMO systems," *IEEE Transactions on Wireless Communications*, vol. 17, no. 9, pp. 5975–5990, Sep. 2018. [Online]. Available: http://arxiv.org/abs/1710.10830

[4] H. Wei, D. Wang, H. Zhu, J. Wang, S. Sun, and X. You, "Mutual coupling calibration for multiuser massive MIMO systems," *IEEE Trans. on Wireless Commun.*, vol. 15, no. 1, pp. 606–619, 2016.

[5] C. Shepard, H. Yu, N. Anand, E. Li, T. Marzetta, R. Yang, and L. Zhong, "Argos: Practical many-antenna base stations," in *Proceedings of the 18th annual international conference on Mobile computing and networking*. ACM, 2012, pp. 53–64.

[6] R. Rogalin, O. Y. Bursalioglu, H. Papadopoulos, G. Caire, A. F. Molisch, A. Michaloliakos, V. Balan, and K. Psounis, "Scalable synchronization and reciprocity calibration for distributed multiuser mimo," *IEEE Transactions on Wireless Communications*, vol. 13, no. 4, pp. 1815–1831, 2014.

[7] R. Rogalin, O. Y. Bursalioglu, H. C. Papadopoulos, G. Caire, and A. F. Molisch, "Hardware-impairment compensation for enabling distributed large-scale mimo," in *2013 Information Theory and Applications Workshop (ITA)*. IEEE, 2013, pp. 1–10.

[8] J. Vieira, F. Rusek, O. Edfors, S. Malkowsky, L. Liu, and F. Tufvesson, "Reciprocity calibration for massive mimo: Proposal, modeling, and validation," *IEEE Transactions on Wireless Communications*, vol. 16, no. 5, pp. 3042–3056, 2017.

[9] H. Papadopoulos, O. Y. Bursalioglu, and G. Caire, "Avalanche: Fast rf calibration of massive arrays," in *2014 IEEE Global Conference on Signal and Information Processing (GlobalSIP)*. IEEE, 2014, pp. 607–611.